^{187}Re(γ, n) cross section close to and above the neutron threshold

S. Müller,* A. Kretschmer, K. Sonnabend, A. Zilges, and D. Galaviz†
Institut für Kernphysik, Technische Universität Darmstadt, Schlossgartenstrasse 9, D-64289 Darmstadt, Germany
(Received 25 February 2005; published 14 February 2006)

The neutron capture cross section of the unstable nucleus ^{186}Re is studied by investigating the inverse photodisintegration reaction ^{187}Re(γ, n). The special interest of the s-process branching point ^{186}Re is related to the question of possible s-process contributions to the abundance of the r-process chronometer nucleus ^{187}Re. We use the photoactivation technique to measure photodisintegration rates. Our experimental results are in good agreement with two different statistical model calculations. Although the cross sections predicted by both models for the inverse reaction ^{186}Re(n, γ) is too low to remove the overproduction of ^{186}Os; the two predicted neutron-capture cross sections differ by a factor of 2.4; this calls for future theoretical study.

DOI: 10.1103/PhysRevC.73.025804 PACS number(s): 26.20.+f, 25.40.Lw, 25.20.Dc, 27.70.+q

I. INTRODUCTION

Almost all elements above mass $A \approx 60$ can be produced in neutron capture reactions [1]. Two different neutron induced processes are necessary to explain the abundance distribution of heavy elements. The first one is the slow neutron capture process (s process). The neutron densities are of the order of $n_n \approx 10^8\,\mathrm{cm}^{-3}$ and the time scale τ_n between two subsequent neutron capture reactions is typically of the order of years. The s-process path propagates along the valley of stability. Whenever an unstable nucleus with a mean lifetime $\tau \ll \tau_n$ is reached, this nucleus β decays. If $\tau \approx \tau_n$, a branching occurs and the s-process path splits. Thus, nuclei with $\tau \approx \tau_n$ are called branching points of the s process. The second process is the rapid neutron capture process (r process). High neutron densities ($n_n \gg 10^{20}\,\mathrm{cm}^{-3}$) lead to the production of very neutron rich nuclei up to 20 mass units away from stable nuclei. During freeze out, these nuclei β decay back to the valley of stability.

There are at least two scenarios known where the s process takes place. It occurs during helium burning in red giant stars and during helium shell flashes in low mass asymptotic giant branch (AGB) stars [2,3]. The former scenario is mainly responsible for the production of elements between iron and yttrium. The latter, for the production of elements between zirconium and bismuth. For a detailed discussion see, e.g., Ref. [4]. In the following we will focus on the mass region $A \approx 185$ and, hence, restrict our discussion to the so-called main component of the s process.

Due to its very long half-life ($t_{1/2} = 5 \times 10^{10}$ a) the nucleus ^{187}Re can be used as a r-process chronometer [8,9]. The ratio $N(^{187}\mathrm{Re})/N_c(^{187}\mathrm{Os})$ is related to the starting point of the r-process in our galaxy and, hence, to its age. N denotes the total and N_c the cosmoradiogenic part of the abundance stemming from the decay of ^{187}Re. To extract the cosmoradiogenic part of the ^{187}Os abundance one has to subtract the s-process abundance N_s from the total abundance N. In Fig. 1 the s-process flow through the W-Re-Os isotopes is shown. The s-process abundance of ^{187}Os can be derived from the abundance of the neighboring s-only nucleus ^{186}Os via the local approximation [10]:

$$N_s(^{187}\mathrm{Os})/N_s(^{186}\mathrm{Os}) \approx F\,\bar{\sigma}_n(^{186}\mathrm{Os})/\bar{\sigma}_n(^{187}\mathrm{Os}), \qquad (1)$$

where $\bar{\sigma}_n$ are the Maxwellian-averaged radiative neutron capture cross sections (MACS) from the ground state, and F accounts for the correction of the cross section due to neutron capture on thermally excited states in ^{187}Os, in particular on the first excited state at 9.75 keV. This correction factor was first calculated in Ref. [11] (see Ref. [12] for discussion). The neutron capture cross sections of ^{186}Os and ^{187}Os were measured by Browne and Berman [9], Browne, Lamaze and Schroder [13], by Browne and Berman [14] and Winters and Macklin [15], resulting in an uncertainty of about 20% for the ratio $R = \bar{\sigma}_n(^{186}\mathrm{Os})/\bar{\sigma}_n(^{187}\mathrm{Os})$. Recently, these cross sections were measured by the n_TOF Collaboration [16,17].

The use of the Re/Os clock is not free of problems. First of all, the half-life of ^{187}Re strongly depends on temperature and ^{187}Os becomes unstable under stellar conditions [5–7]. Thus, it is necessary to use chemical evolution models of the galaxy [6] to include irradiation effects on the abundance ratio R. The two branchings at ^{185}W and ^{186}Re also affect the s-process abundances in this region. Finally, the $N_s\bar{\sigma}_n$ correlation from Eq. (1) for the two s-only isotopes ^{186,187}Os is not fulfilled. This can be caused by two facts. Either the branchings are not correctly modeled or the capture cross sections are strongly affected by stellar conditions. The branching at ^{185}W has already been studied and an overproduction of ^{186}Os was reported due to the new experimental value [18]. Thus the radiative neutron capture cross section of ^{186}Re is the only relevant cross section in this mass region which is not known experimentally yet.

In this paper we study the radiative neutron capture cross section of the branching point nucleus ^{186}Re using an indirect method. The unstable nucleus ^{186}Re decays via β^--decay to ^{186}Os or via electron capture to ^{186}W with a half-life of $t_{1/2} = 3.7$ d. Due to the fact that neutron capture experiments with such short-lived targets are nearly impossible, we choose the inverse reaction ^{187}Re(γ, n)^{186}Re for our investigation.

*Electronic address: mueller@ikp.tu-darmstadt.de
†Present address: NSCL, Michigan State University, 1 Cyclotron Lab, East Lansing, MI 48824-1321, USA.

 ©2006 The American Physical Society

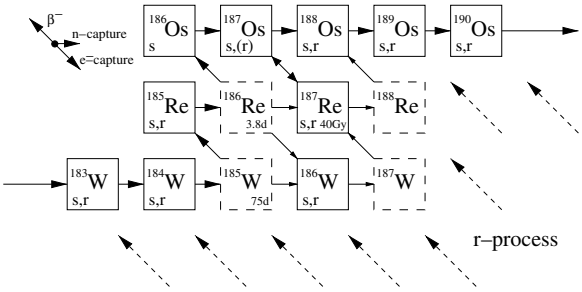

FIG. 1. The s-process path in the W-Re-Os mass region. Unstable nuclei are marked by dashed boxes (except ^{187}Re). The indicated values are laboratory half-lives. However, the half-life of ^{187}Re decreases by 10 orders of magnitude at typical s-process temperatures of $T = 3 \times 10^8$ K and ^{187}Os becomes unstable [5–7].

After neutron emission the ^{186}Re nucleus is in the ground state or some excited state and the measured cross section is a sum over several channels. With maximum excitation energies just above the neutron threshold, only the lowest states can be reached, e.g., the first excited state in ^{186}Re at 59 keV. On the other hand, these low lying states in the ^{186}Re nucleus are also thermally populated—however, not in the same proportions—under s-process conditions and contribute to the neutron capture cross section. Thus, the ^{187}Re$(\gamma, n)^{186}$Re cross section and the cross section of the inverse reaction ^{186}Re$(n, \gamma)^{187}$Re are related via the principle of detailed balance.

In Sec. II we describe our experimental setup. Section III explains the analysis of our data and the results for the ^{187}Re(γ, n) cross section are presented. The results are compared to calculations using the NON-SMOKER [19,20] and MOST [21,22] codes. Both computer codes are based on the statistical Hauser-Feshbach model but use different input parameters. In Sec. IV the implications on the Re/Os clock are briefly discussed.

II. EXPERIMENTAL SETUP

The ^{187}Re$(\gamma, n)^{186}$Re experiment was performed using the photoactivation technique at the real photon setup [23] at the superconducting electron accelerator S-DALINAC [24] at Darmstadt University of Technology (see Fig. 2). The monoenergetic electron beam hits a thick copper radiator ($d \approx 1.4$ cm), where it is completely stopped and converted into a continuous spectrum of bremsstrahlung photons with an endpoint energy $E_{\max}$. The photons are collimated and irradiate the target of interest at a distance of $d \approx 150$ cm behind the radiator. This leads to a well-defined photon beam with a spectral composition that is analyzed in detail, see, e.g., Ref. [25]. The γ-intensity as well as the electron current are monitored online in order to control the beam position on the copper radiator. The targets consist of thin metallic rhenium discs ($m \approx 340$ mg, $\emptyset = 2$ cm) of natural isotopic composition and of two layers of boron ($m \approx 650$ mg each, $\emptyset = 2$ cm) embedding the rhenium disk with a sandwich-like structure. The incoming photon intensity is normalized using the nuclear resonance fluorescence reaction ^{11}B(γ, γ') [26] (see Fig. 3). The scattered photons are registered online with

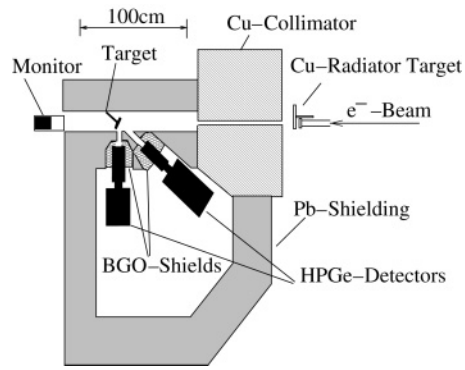

FIG. 2. The real photon setup at the superconducting electron accelerator S-DALINAC at Darmstadt University of Technology. The electron beam with a maximum energy of 10 MeV and maximum intensity of 40 μA hits a thick copper target and produces bremsstrahlung. The beam position is monitored with an ionization chamber. The flux is monitored online with two actively shielded 100% HPGe detectors using the ^{11}B(γ, γ') reaction.

two HPGe detectors positioned at 90° and 130° with respect to the beam direction. The detector efficiency ϵ was measured up to 3.6 MeV using standard calibration sources. We have used the Monte Carlo code GEANT [27] to extrapolate the efficiencies up to an energy of 10 MeV.

The spectral photon distribution was simulated with the same code and is adjusted to the photon intensities obtained from the ^{11}B(γ, γ') reaction. The result for the case $E_{\max} = 9.9$ MeV is shown in Fig. 3. A list of all measured energies is shown in Table I. The statistic uncertainty for the photon flux calibration is very small because of the well-known photoresponse of ^{11}B [28]. The systematic uncertainty includes a 5% uncertainty from the detector efficiency extrapolation to higher energies and the uncertainty due to the shape of the photon spectrum close to the endpoint energy. This uncertainty is smaller for higher endpoint energies because the γ transitions at 8.92 MeV in the reaction ^{11}B(γ, γ') can be used for calibration if $E_{\max} > 9$ MeV. The total uncertainty for the photon flux calibration can be estimated to be about 12% to 21% depending on the endpoint energy $E_{\max}$ (see Table II).

After activation, the γ-rays from the decay of the unstable nucleus produced are measured offline using a well shielded

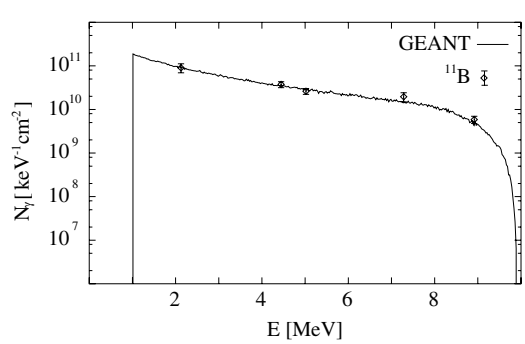

FIG. 3. Adjustment of the simulated spectral photon distribution to the intensities N_γ obtained from the reaction ^{11}B(γ, γ') at $E_{\max} = 9.9$ MeV. The flux is integrated over 23 h, a typical activation time.

TABLE I. The peak area Y of the two γ-transitions following the β-decay of ^{186}Re and the corresponding number of (γ, n)-reactions $\mathcal{R}$. The results for the transition at 122 keV at $E_{\max} = 7.65$ MeV are omitted due to low statistics.

$E_{\max}$ [MeV]	Y(122 keV) [10^3]	Y(137 keV) [10^3]	$\mathcal{R}$(122 keV) [10^6]	$\mathcal{R}$(137 keV) [10^6]
9.9	35.12 ± 0.22	605.7 ± 0.8	287 ± 14	286 ± 14
9.45	17.48 ± 0.15	301.3 ± 0.6	148 ± 8	147 ± 7
9.0	9.91 ± 0.20	167.6 ± 0.4	85.0 ± 4.6	83.0 ± 4.2
8.55	3.36 ± 0.07	58.81 ± 0.25	33.7 ± 1.8	34.1 ± 1.7
8.325	1.79 ± 0.05	29.66 ± 0.18	16.3 ± 1.0	15.6 ± 0.8
8.1	0.87 ± 0.04	14.98 ± 0.18	6.86 ± 0.48	6.85 ± 0.35
7.875	0.50 ± 0.04	7.62 ± 0.09	3.24 ± 0.31	2.85 ± 0.15
7.65		6.82 ± 0.08		0.39 ± 0.02

HPGe detector with an energy resolution better than 0.15% and an efficiency of 30% relative to a 3 in. × 3 in. NaI detector. The detector efficiency is determined between 60 keV and 1.3 MeV with standard calibration sources. The target geometry and self absorption effects are simulated with a Monte Carlo code [27]. A typical spectrum after activation is shown in Fig. 4.

The peak area Y is directly proportional to the number of (γ, n)-reactions $\mathcal{R}$ in the target during the activation. Knowing the detector efficiency ϵ and the absolute γ-branching of the transition, the factor of proportionality can be directly calculated for each run using the law of exponential decay. The number of (γ, n)-reactions $\mathcal{R}$ is proportional to the energy-integrated cross section I_σ,

$$\mathcal{R} = n_t\, I_\sigma = n_t \int_{S_n}^{E_{\max}} N_\gamma(E, E_{\max})\sigma(E)\, dE, \qquad (2)$$

where n_t is the number of ^{187}Re atoms, S_n is the neutron threshold, $E_{\max}$ is the energy of the electron beam and, hence, the endpoint energy of the spectral density distribution $N_\gamma(E, E_{\max})$ of the bremsstrahlung photons, and $\sigma(E)$ is the ^{187}Re(γ, n)^{186}Re cross section. We used the strong transitions at 137 and 122 keV, respectively, for our analysis.

The uncertainty of I_σ is about 5% to 6%. The statistical uncertainty is small due to the high sensitivity of the photoactivation technique (see Fig. 4). The uncertainty of I_σ is dominated by the 5% uncertainty stemming from the simulation of the detector efficiency including self-absorption effects in the target. The peak areas Y and the number of (γ, n)-reactions $\mathcal{R}$ are summarized in Table I. The different components of the uncertainties as well as the total uncertainty are summarized in Table II for each endpoint energy $E_{\max}$.

TABLE II. Summary of experimental uncertainties for the different endpoint energies $E_{\max}$. The details are discussed in the text.

	γ-intensity		number of (γ, n)-reactions			
$E_{\max}$ [keV]	stat. [%]	sys. [%]	shape [%]	stat. [%]	sys. [%]	Total [%]
9900	1.0	9.8	8	0.1	5	13.6
9450	1.4	8.6	8	0.2	5	12.8
9000	1.2	10.7	11	0.2	5	16.2
8550	1.3	12.9	11	0.4	5	17.7
8325	1.5	10.7	11	0.6	5	16.2
8100	2.0	14.1	14	0.8	5	20.6
7875	1.8	14.9	14	1.2	5	21.2
7650	2.0	13.0	14	1.2	5	19.9

III. ANALYSIS OF THE DATA

The peak area in the activation spectrum is only proportional to I_σ, thus, we cannot determine the cross section directly. Assuming a certain shape of the cross section, one can verify and normalize this assumption by measuring at several endpoint energies because the centroid of the integrand in Eq. (2) changes for each endpoint energy.

In case of pure s-wave neutron emission, the (γ, n) cross section can be parametrized as [29]

$$\sigma(E) = \sigma_0 \sqrt{\frac{E - S_n}{S_n}} \qquad (3)$$

for the energy region close above the neutron threshold energy $S_n(^{187}\text{Re}) = 7.363$ MeV. The combination of Eq. (3) with Eq. (2) yields the normalization factor σ_0. The normalization factors shown in Fig. 5 as a function of endpoint energy should be constant. We have measured the integrated cross

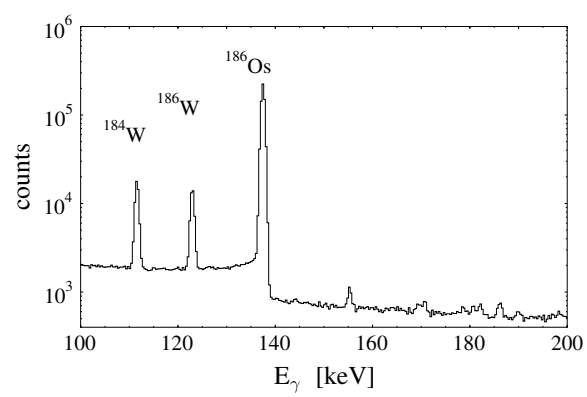

FIG. 4. Typical γ-spectrum measured after photoactivation of ^{nat}Re. The line at 122 keV and at 137 keV stem from the β-decay of ^{186}Re into ^{186}W and ^{186}Os, respectively. The line at 111 keV stems from the decay of ^{184}Re into ^{184}W. The target was activated for 23 h at an energy of $E_{\max} = 9.9$ MeV and the γ-spectrum was accumulated over a period of 23 h starting 1 h after activation.

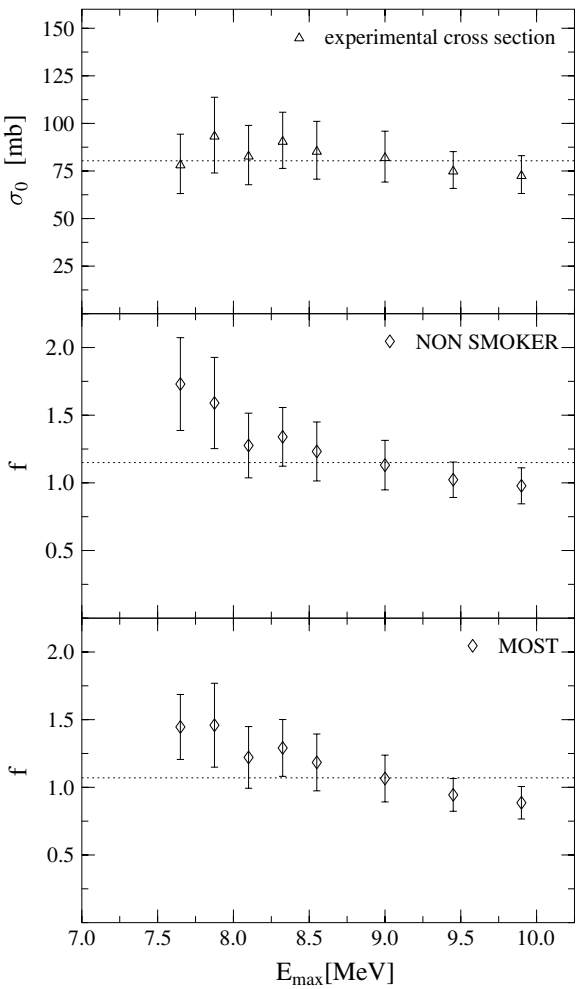

FIG. 5. The normalization factors σ_0 of Eq. (3), alternatively f of Eq. (6) are shown as a function of the endpoint energy E_{max} of the photon spectrum for our experimental cross section and for the two theoretical predicted cross sections. Both model predictions seem to underestimate the cross section slightly in the vicinity of the reaction threshold.

section using bremsstrahlung with endpoint energies of 7.65, 7.875, 8.1, 8.325, and 8.55 MeV, respectively. For $S_n < E < 8.55$ MeV we obtain

$$\sigma(E) = (80.4 \pm 9.6)\,\mathrm{mb}\sqrt{\frac{E - S_n}{S_n}}. \tag{4}$$

Between 9.5 and 19 MeV, the (γ, n) cross section can be parametrized by a superposition of two Lorentzians [30]. Between 8.55 and 9.5 MeV, we interpolate the cross section with a third order polynomial. The requirement that the cross section as well as its first derivative are continuous, determines the four parameters of the polynomial:

$$\left(\frac{\sigma(E)}{\mathrm{mb}}\right) = -17\left(\frac{E}{\mathrm{MeV}}\right)^3 + 4.7\times 10^2\left(\frac{E}{\mathrm{MeV}}\right)^2 - 4.3\times 10^3\left(\frac{E}{\mathrm{MeV}}\right) + 1.3\times 10^4. \tag{5}$$

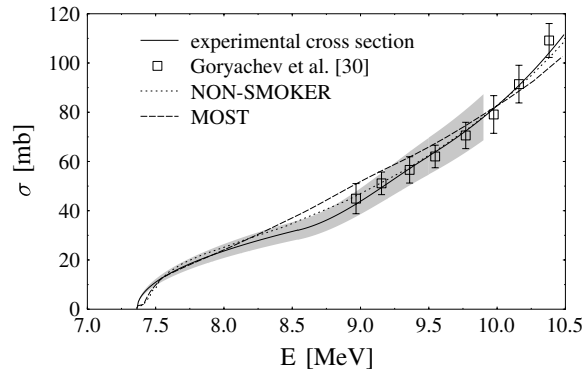

FIG. 6. Comparison of the experimental ^{187}Re(γ, n) cross section to the calculated cross sections from the MOST and NON-SMOKER codes. Additionally, the data points extracted from Goryachev *et al.* [30] are plotted. The shaded area represents the uncertainty of our experimental results.

The parametrization of the cross section for the energy range between S_n and 10.5 MeV is shown in Fig. 6. The measurements performed at $E_{max} = 9.0$, 9.45 and 9.9 MeV verify this parametrization up to the low energy tail of the giant dipole resonance. Our data fit nicely with an older experiment [30], in which the ^{187}Re(γ, n) cross section was measured at higher energies around the giant dipole resonance.

Alternatively one can start with a cross section σ_{th} calculated with the NON-SMOKER or MOST code. A normalization factor f is introduced for absolute calibration:

$$I_\sigma = f \cdot \int_{S_n}^{E_{max}} \sigma_{th}(E) N_\gamma(E, E_{max})\, dE. \tag{6}$$

The normalization factor f needs to be energy independent presuming that the predicted shape of the cross section σ_{th} is correct. Additionally, if the absolute value of the calculated cross section is correct, f should be close to 1.0. The normalization factors f are determined to be

$$f_{NONS} = 1.15 \pm 0.31, \tag{7}$$

$$f_{MOST} = 1.07 \pm 0.28. \tag{8}$$

The normalization factors as a function of the endpoint energy E_{max} are shown in Fig. 5 and the normalized cross sections are shown in Fig. 6. The agreement between the two calculations and our experimental cross section is remarkably good. The small deviations in the threshold region result either from experimental uncertainties regarding the precise shape of the bremsstrahlung close to the endpoint energy E_{max} or from numerical problems occurring in the theoretical calculation.

IV. IMPLICATIONS FOR THE RE/OS CLOCK

The current uncertainty of the time duration of nucleosynthesis obtained from the Re/Os clock is about 2.3 Gyr [31]. The main source of uncertainty with regard to nuclear physics aspects of the clock are presently the neutron capture cross sections.

TABLE III. The MACS calculated with an updated version of NON-SMOKER [20] and MOST [21] for a typical s-process temperature of $kT = 30$ keV. The stellar enhancement factor as well as the adopted values of the MACS were taken from Bao *et al.* [32].

	σ_{GS} [mb]	$\sigma_{thermal}$ [mb]
NON-SMOKER [20]	1485	1546
MOST [21]	616	623
Ref. [32]	1550 ± 250	1615 ± 260

The Maxwellian-averaged neutron capture cross sections in Table III are derived using the MOST and NON-SMOKER codes. The (γ, n) cross sections are in good agreement with the present experimental results (see Fig. 6). However, the neutron capture cross sections of the inverse reaction differ by a factor of 2.4.

Taking the value recommended by Bao *et al.* [32] the branching ratio between β-decay and neutron capture is $R = \lambda_n/\lambda_\beta = 5.4 \times 10^{-4}$. Considering the values from the NON-SMOKER and MOST calculations, one obtains $R_{NONS} = 5.2 \times 10^{-4}$ and $R_{MOST} = 2.1 \times 10^{-4}$, respectively. Both models predict a (n, γ)-cross section which is smaller than the value recommended in Ref. [32]. This would lead to a further enhanced production of ^{186}Os. Nevertheless due to the small branching the abundance distribution of the elements in this mass region is not changed significantly.

V. SUMMARY AND CONCLUSION

We have measured the ^{187}Re(γ, n) cross section just above the reaction threshold. The cross sections calculated within the statistical model using the computer codes NON-SMOKER and MOST are in good agreement with our experimental data. Even though the predictions for the photodisintegration cross sections are nearly identical, the MACS for the neutron capture reactions differ by a factor of 2.4. At this point, further theoretical investigations are necessary.

The MACS calculated with the updated NON-SMOKER code is close to the value given in Ref. [32]. Thus, the overproduction of ^{186}Os reported in Ref. [18] remains. The MACS calculated with the MOST code is significantly lower and, therefore, a further increase of the ^{186}Os production is predicted. For a more quantitative statement, complex network calculations are mandatory.

The disagreement between the two models may have its origin in the lack of precise nuclear data that enter into both models. This shows again the need for high precision mass measurements, $E1$-strength distribution studies, and the study of nucleon-nucleus optical potentials.

The fact that both model predictions are in good agreement with our data but could not reduce the overproduction of ^{186}Os supports the idea that the adopted value of the ^{186}Os(n, γ) cross section [32] is too small. Very recent results from an experiment at the n-TOF facility at CERN [16] and at the Forschungszentrum Karlsruhe [17] point in this direction as well.

ACKNOWLEDGMENTS

We thank S. Goriely and T. Rauscher for performing the calculations with the MOST and NON-SMOKER codes, respectively. We thank the S-DALINAC group around H.-D. Gräf for their support during the experiment and the members of our group, especially M. Babilon, W. Bayer, K. Lindenberg, D. Savran, and S. Volz for their help during the beam time. We thank F. Käppeler, T. Shizuma, and H. Utsunomiya for encouraging discussions. We thank F. Käppeler for a careful reading of the manuscript. We thank P. Mohr for initiating this experiment and for discussions. This work was supported by the Deutsche Forschungsgemeinschaft under contract SFB 634.

[1] E. Burbidge, G. Burbidge, W. Fowler, and F. Hoyle, Rev. Mod. Phys. **29**, 547 (1957).
[2] F. Käppeler, R. Gallino, M. Busso, G. Picchio, and C. Raiteri, Astrophys. J. **354**, 630 (1990).
[3] C. Arlandini, F. Käppeler, K. Wisshak, R. Gallino, M. Lugaro, M. Busso, and O. Straniero, Astrophys. J. **525**, 886 (1999).
[4] G. Wallerstein, I. Iben, P. Parker, A. M. Boesgaard, G. M. Hale, A. E. Champagne, C. A. Barnes, F. Käppeler, V. V. Smith, R. D. Hoffman *et al.*, Rev. Mod. Phys. **69**, 995 (1997).
[5] F. Bosch, T. Faestermann, J. Friese, F. Heine, P. Kienle, E. Wefers, K. Zeitelhack, K. Beckert, B. Franzke, O. Klepper *et al.*, Phys. Rev. Lett. **77**, 5190 (1996).
[6] K. Yokoi, K. Takahashi, and M. Arnould, Astron. Astrophys. **117**, 65 (1983).
[7] K. Takahashi and K. Yokoi, Nucl. Phys. **A404**, 578 (1983).
[8] D. D. Clayton, Astrophys. J. **139**, 637 (1964).
[9] J. C. Browne and B. L. Berman, Nature (London) **262**, 197 (1976).
[10] D. D. Clayton, W. A. Fowler, T. E. Hull, and B. A. Zimmermann, Ann. Phys. (NY) **12**, 331 (1961).
[11] S. E. Woosley and W. A. Fowler, Astrophys. J. **233**, 411 (1979).
[12] M. Arnould, K. Takahashi, and K. Yokoi, Astron. Astrophys. **137**, 51 (1984).
[13] J. C. Browne, G. P. Lamaze, and I. G. Schroder, Phys. Rev. C **14**, 1287 (1976).
[14] J. C. Browne and B. L. Berman, Phys. Rev. C **23**, 1434 (1981).
[15] R. R. Winters and R. L. Macklin, Phys. Rev. C **25**, 208 (1982).
[16] M. Mosconi, A. Mengoni, M. Heil, F. Käppeler, G. Aerts, R. Terlizzi, U. Abbondanno, H. Alvarez, F. Alvarez-Velarde, S. Andriamonje *et al.*, in *AIP Conf. Proc. 769: International Conference on Nuclear Data for Science and Technology (2005)*, pp. 1335–1338.
[17] F. Käppeler, in press (2005).
[18] K. Sonnabend, P. Mohr, K. Vogt, A. Zilges, A. Mengoni, T. Rauscher, H. Beer, F. Käppeler, and R. Gallino, Astrophys. J. **583**, 506 (2003).
[19] T. Rauscher and F.-K. Thielemann, At. Data Nucl. Data Tables **75**, 1 (2000).

[20] T. Rauscher and F.-K. Thielemann, At. Data Nucl. Data Tables **88**, 1 (2004).
[21] M. Aikawa, M. Arnould, S. Goriely, A. Jorissen, and K. Takahashi, Astron. Astrophys. **441**, 1195 (2005).
[22] S. Goriely and E. Khan, Nucl. Phys. **A706**, 217 (2002).
[23] P. Mohr, J. Enders, T. Hartmann, H. Kaiser, D. Schiesser, S. Schmitt, S. Volz, F. Wissel, and A. Zilges, Nucl. Instrum. Methods A **423**, 480 (1999).
[24] A. Richter, in *Proceedings of Fifth European Particle Accelerator Conference*, Barcelona, 1996, edited by S. Myers *et al.* (IOP, Bristol, 1996), p. 110.
[25] K. Vogt, P. Mohr, M. Babilon, J. Enders, T. Hartmann, C. Hutter, T. Rauscher, S. Volz, and A. Zilges, Phys. Rev. C **63**, 055802 (2001).
[26] P. Mohr, T. Hartmann, K. Vogt, S. Volz, and A. Zilges, in *AIP Conf. Proc. 610: Nuclear Physics in the 21st Century (2002)*, p. 870.
[27] R. Brun and F. Carminati, GEANT Detector Description and Simulation Tool, CERN Program Library Long Writeup **W5013** edition (CERN, Geneva, 1993).
[28] F. Ajzenberg-Selove, Nucl. Phys. **A506**, 1 (1990).
[29] H. A. Bethe, Rev. Mod. Phys. **9**, 69 (1937).
[30] A. M. Goryachev, G. N. Zalesnyie, S. F. Semenko, and B. A. Tulupov, Sov. J. Nucl. Phys. **17**, 236 (1973).
[31] A. Mengoni and F. Käppeler, in *AIP Conf. Proc. 561: Symposium on Nuclear Physics IV (2001)*, p. 72.
[32] Z. Y. Bao, H. Beer, F. Käppeler, F. Voss, K. Wisshak, and T. Rauscher, At. Data Nucl. Data Tables **76**, 70 (2000).